Liquid Crystals
Publication details, including instructions for authors and subscription information:
http://www.informaworld.com/smpp/title~content=t713926090

Effect of a biphenyl side chain of polyimide on the pretilt angle of liquid crystal molecules: molecular simulation and experimental studies

Ming Li[a]; Hua Lai[a]; Boxun Chen[b]; Xiangyang Liu[a]; Yi Gu[a]
[a] State Key Laboratory of Polymer Materials and Engineering, College of Polymer Science and Engineering, Sichuan University, Chengdu, China [b] College of Computer Science, Sichuan University, Chengdu, China

Online publication date: 11 February 2010

To cite this Article Li, Ming , Lai, Hua , Chen, Boxun , Liu, Xiangyang and Gu, Yi(2010) 'Effect of a biphenyl side chain of polyimide on the pretilt angle of liquid crystal molecules: molecular simulation and experimental studies', Liquid Crystals, 37: 2, 149 — 158
To link to this Article: DOI: 10.1080/02678290903420234
URL: http://dx.doi.org/10.1080/02678290903420234

Liquid Crystals,
Vol. 37, No. 2, February 2010, 149–158

Taylor & Francis
Taylor & Francis Group

Effect of a biphenyl side chain of polyimide on the pretilt angle of liquid crystal molecules: molecular simulation and experimental studies

Ming Li[a], Hua Lai[a], Boxun Chen[b], Xiangyang Liu[a] and Yi Gu[a]*

[a]*State Key Laboratory of Polymer Materials and Engineering, College of Polymer Science and Engineering, Sichuan University, Chengdu 610065, China;* [b]*College of Computer Science, Sichuan University, Chengdu 610065, China*

(Received 23 July 2009; revised 16 October 2009)

The side chain structure of polyimides (PIs) exerts an important effect on the pretilt angle of liquid crystal molecules. Three PIs with different side chain structures were prepared based on 3,3′,4,4′-biphenyl dianhydride (BPDA) and 1,3-phenylene diamine (*m*-PDA), 3,5-diaminobenzoic-4′-biphenyl ester (DABBE) and 4′-(*tert*-butyldimethylsiloxy) biphenyl-4-yl 3,5-diaminobenzoate (DPA). The surface properties of the PI films and the pretilt angles of the liquid crystal molecules on them were examined with experimental and molecular simulation methods, showing a good agreement between two methods. Molecular simulation showed that the BPDA-DPA system had the lowest surface energy for its side chain enriched on the PI surface, which was driven by the low polar silyl end group of side chain. The phenyl ring in the PI backbone tended to be arranged parallel with the surface, while the phenyl ring in the side chain inclined to align vertical to surface. By incorporation of the biphenyl group and the silyl end group, the pretilt angle of the PI increased from 3° to 89°. This was attributed to the enrichment degree of the side chain on the surface and the configuration of the biphenyl group in the side chain. The main interactions between the liquid crystal molecule, 4-*n*-pentyl-4′ -cyanobiphenyl (5CB) and the PIs was a π–π interaction between the biphenyl group in 5CB and the PIs.

Keywords: polyimide; side chain; molecular dynamics simulation; liquid crystal; surface enrichment

1. Introduction

A liquid crystal display (LCD) device is composed of several materials, such as liquid crystals (LCs), a colour filter and a LC alignment layer. The LC alignment layer plays an important role in aligning the LC molecules uniformly and inducing pretilt angle [1], a parameter greatly influencing the LCD's performance. The alignment layer is usually made of polyimide (PI) film processed by rubbing [2] or photoaligning [3,4]. However, a high pretilt angle cannot be obtained by main-chain PIs. The incorporation of special side chains in many studies was a major method to increasing the pretilt angle [5–15]. However, the type of side chains, alkyl [7–9], fluoroakyl [10] or alkyl-endcapped aryl groups [5, 6, 11–15] tremendously varied the obtained pretilt angle; in particular, the vertical pretilt angle could be implemented by the introduction of alkyl-endcapped aryl groups. Lee *et al.* [5] studied the effect of side chain flexibility on the pretilt angle and found that only a PI with a side chain of rigid alicyclic structure and 6-methylheptyl flexible end group could maintain the high pretilt angle for 86°, even after the rubbing process. Liu *et al.* [14] synthesised a series of PIs with side chains containing rigid biphenyl structures and non-polar alkoxy end groups. When the number of carbons in the alkoxy groups increased to six, the vertical pretilt angle was obtained. In our group, a novel polyimide pendent with 4′-(*tert*-butyldimethylsiloxy) biphenyl-4-yl group generated vertical alignment [15]. Why do side chain structures generate different pretilt angles and how can they be controlled? So far, little research has been done in this field because of the lack of a useful tool to characterise the interaction between the PI surface and the LC molecules. In the present research, we applied the molecular simulation method to study the effect of the side chain structure of PIs on the pretilt angle of liquid molecules [16]. The PI polymerised from 3,3′,4,4′-biphenyl dianhydride (BPDA) and 4′-(*tert*-butyldimethylsiloxy) biphenyl-4-yl 3,5-diaminobenzoate (DPA) reported in [15] was prepared and characterised by experimental and molecular simulation methods. For comparison, we also prepared the PIs based on 3,5-diaminobenzoic-4′-biphenyl ester (DABBE) without a low polar group, and the backbone diamine 1,3-Phenylene diamine (*m*-PDA), which were polymerised with BPDA. The chemical structures of the three systems are shown in Figure 1.

In this study, we used molecular mechanic (MM) and molecular dynamic (MD) simulations to determine the surface energy and configuration of the three PI systems. Then, we studied the interactions between the PI alignment layers and the LCs by performing MD simulations of two systems: (i) a single 4-*n*-pentyl-4′-cyanobiphenyl (5CB) LC molecule; and

*Corresponding author. Email: guyi@scu.edu.cn.

ISSN 0267-8292 print/ISSN 1366-5855 online

DOI: 10.1080/02678290903420234
http://www.informaworld.com

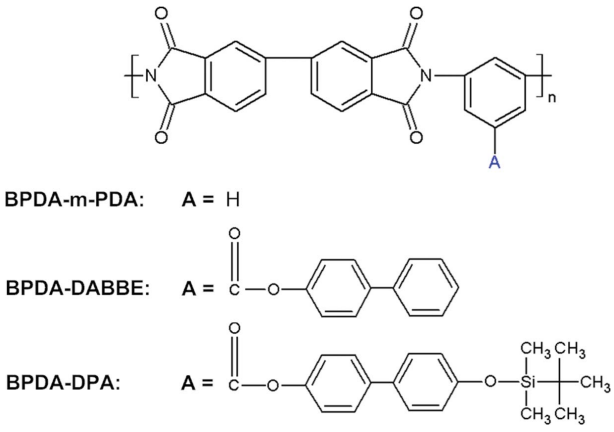

Figure 1. Chemical structures of the three PI systems: BPDA-*m*-PDA, BPDA-DABBE and BPDA-DPA.

(ii) a monolayer of 5CB molecules. The results of the pretilt angle showed a good agreement with the experimental value, and the mechanism for LC alignment was discussed as an initial study.

2. Experimental

2.1 Materials and preparation

DPA and DABBE were synthesised in our lab as reported in [15, 17]. *m*-PDA was purified by sublimation. BPDA (Acros Organics, New Jersey) was dried for 5 h at 180°C prior to use. *N*-Methyl-2-pyrrolidinone (NMP, Pu Yang MYJ Technology, China) was distilled under reduced pressure after being dried by P_2O_5. 4-pentyl-4′-cyanobiphenyl (5CB) was supplied by the Beijing Tsinghua Yawang Liquid Crystal Materials Co., Ltd, China.

The PIs, BPDA-*m*-PDA, BPDA-DABBE and BPDA-DPA, were prepared by the conventional two-step method. Firstly, a poly(amic acid) was synthesised by adding solid BPDA to a solution of recrystallised diamine in freshly distilled NMP. The molar ratio of dianhydride and diamine was maintained at 1:1. The reaction mixture was stirred at 0°C for 12 h with nitrogen flow to give a yellow poly(amic acid) solution. Then the solution were spin coated on indium tin oxide (ITO)-coated glass plates at 500 rpm for 5 s and 1500 rpm for 10 s, respectively, followed by thermal imidisation under 230°C and 300°C each for 1 h.

2.2 Measurement

The pretilt angle measurement was conducted using the same method in [15]. The prepared PI films were rubbed with a rubbing strength of 57.0 mm. The LC cells were fabricated from two pieces of rubbed PI films assembled in an antiparallel rubbing direction with 43 μm (cell gap) thick spacers and filled with 5CB by the capillary method. The pretilt angles for the fabricated LC cells were measured by a crystal rotation method with a PAT-20 measurement device (Chanchun Liancheng Instrument Co., Ltd.). High pretilt angles near 90° were confirmed by conoscopy using a polarising light microscopy (LEICA DMLP, Germany).

The contact angles of deionised water and methylene iodide on the surface of the PI films were measured by a Krüss DSA100 measurement device (Germany). Each sample was tested three times and the mean contact angles were obtained. A Young's harmonic mean equation was applied to predict the surface energies from the contact angles. X-ray photoelectron spectroscopy (XPS) was conducted using a Kratos ASAM800 spectrometer (England) with AlK_α (1486.6 eV) monochromatised radiation. High-resolution spectra were acquired with pass energy of 10 eV and a take-off angle of 20° [18].

2.3 Molecular simulation

MM and MD simulations were performed using Materials Studio® software [19] by employing the Dreiding [20] force field.

2.3.1 PI thin film

Four PI chains of each system were generated with several monomer units (BPDA-*m*-PDA: 32, BPDA-DABBE: 16, BPDA-DPA: 16). Although the system size of the 16 repeat units is not enough to represent conformations of a real polymer chain, previous researchers have reported reasonable results when they used 10–15 repeat units for PI simulation [21, 22]. Each chain was packed into a cubic cell with a periodic boundary condition, according to Theodorou and Suter's method [23, 24], and minimised by the conjugate gradient method. The relaxation for cells was performed by constant pressure and temperature (*NPT*) ensemble MD simulation from 300 to 700 K for 10 cycles of annealing simulation. The total simulation time was 1 ns. The comparable cell density was obtained, which was about 10% less than the experimental value [25]. The final structure was performed with constant volume and temperature (*NVT*) ensemble MD simulation for 500 ps at 298 K to get the equilibrium configuration.

Thin films were constructed from well-equilibrated cells by elongating the *z*-axis to 10 nm until the parent chain no longer interacted with its image in the *z* direction (Figure 2) [26]. This method had been widely used in the construction of polymer thin film [26–29].

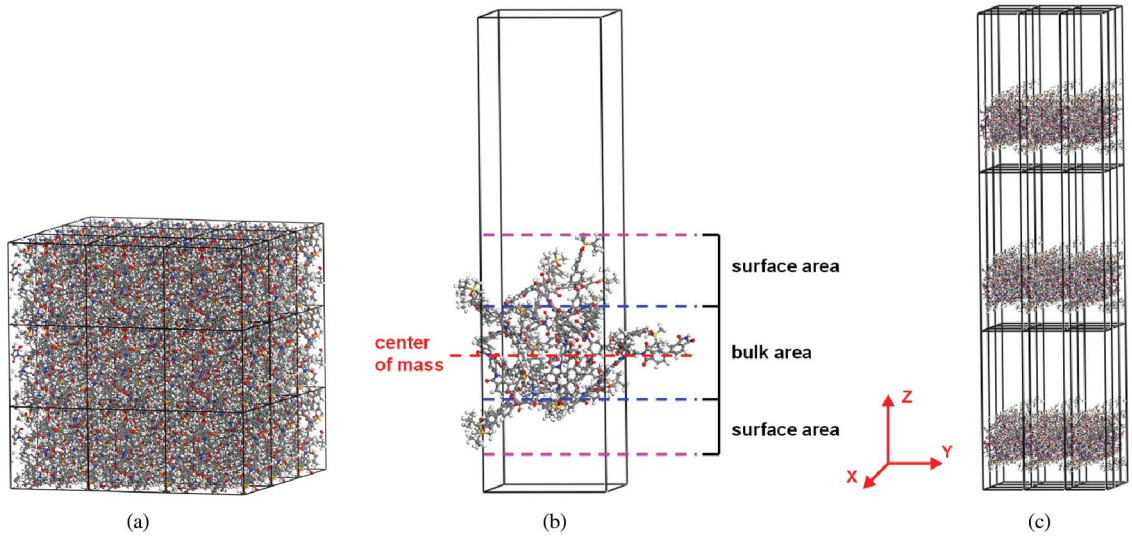

Figure 2. Simulation scheme to prepare a PI thin film: (a) equilibrium bulk phase with periodic boundary conditions; (b) thin film after cell elongation; and (c) multilayered thin films with periodic conditions.

The cell extension resulted in two free surfaces per thin film. The relaxation of the structure formed by conversion of the bulk to film was achieved by MM energy minimisation with the conjugate gradient method, followed by 50 ps *NVT* ensemble MD simulation at 700 K for relaxation. Then, it was further equilibrated by *NVT* ensemble MD simulation for 500 ps at 298 K.

2.3.2 Interactions between PI and liquid crystal molecules

We studied the interactions between the PI alignment layers and LC molecules by performing MD simulations of two systems: (i) a single 5CB molecule; and (ii) a monolayer of 5CB molecules. In both cases the LC molecules were contacted with a PI film, which was discussed in Section 2.3.1.

For single molecule studies, the LC molecule freely explored all orientations on the PI film. The results from 100 simulations in four cells with uniformly distributed starting orientations were combined [30]. Each of the individual simulations was equilibrated for a 200 ps *NVT* ensemble MD simulation at 298 K prior to data collection, which was sufficient to ensure that all memory of the initial orientation was lost. For simulations with a monolayer, we chose the preferred configuration, as indicated by the final structure of the single-molecule simulation. The systems were well equilibrated after a 400 ps *NVT* ensemble MD simulation at 298 K.

In all of the above MD simulations, data collection was carried out for 100 ps, saving the trajectory every 0.5 ps. The temperature and pressure was equilibrated with the Nose thermostat [31, 32] and the Berendsen barostat [33], respectively. The non-bond interactions were calculated in this study with the cut-off being set to 1.05 nm, which was less than half of the cell length.

3. Results and discussion

3.1 Surface properties

3.1.1 Surface energy

The surface energy was calculated from the following:

$$\gamma = \frac{E_{\text{film}} - E_{\text{bulk}}}{2A}, \tag{1}$$

where E_{film} is the average energy of the thin films, E_{bulk} is the average energy of the bulk amorphous cells and A is the surface area that was formed due to the creation of the thin film. The total energy can be decomposed into a bonded portion and a non-bonded portion. The bonded portion consists of energetic terms including bond length (stretch) and bond angle (bend), torsional potential (torsion) and out of plane inversion (oop). The non-bonded portion involves the van der Waals (vdW) and electrostatic (Coulomb) contributions. The contributions of these terms are shown in Table 1 for the three PI systems. The surface energy calculations suggested that the simulation results compared well with the experimental measurements, whose values were BPDA-*m*-PDA (52.3 mJ m^{-2}), BPDA-DABBE (52.0 mJ m^{-2}) and BPDA-DPA (39.3 mJ m^{-2}).

Table 1. Components of internal energy (kJ mol^{-1}) of the BPDA-*m*-PDA, BPDA-DABBE and BPDA-DPA bulk structures and the corresponding thin films with the ensemble-averaged surface energy (γ) expressed in mJ m^{-2}.

	BPDA-*m*-PDA		BPDA-DABBE		BPDA-DPA	
	$\gamma = 56.1$		$\gamma = 52.2$		$\gamma = 42.6$	
	Cell	Film	Cell	Film	Cell	Film
Total	4937.2	5359.7	4444.1	4779.9	3945.1	4277.0
Bond	830.0	813.6	702.7	690.9	835.4	830.6
Angle	5195.7	5136.4	2960.8	2902.2	3360.3	3293.2
Torsion	2536.9	2304.4	2443.0	2182.5	2500.0	2272.9
oop	114.2	52.6	105.9	44.5	118.4	56.4
vdW	2443.2	3118.4	2068.7	2702.6	2399.2	2984.1
Coulomb	–6182.7	–6065.7	–3837.0	–3742.7	–5268.3	–5160.2

Notice that the vdW interaction energy terms contributed considerably to the formation of the free surface of the films. Because of the containing silicon group, which had low surface tension, the simulated surface energy of BPDA-DPA is 42.6 mJ m^{-2}, which was lower than BPDA-*m*-PDA (56.1 mJ m^{-2}) and BPDA-DABBE (52.2 mJ m^{-2}). However, the torsional, bend and bond stretching energies of the films were lower than the bulk cells. The main reason for this was the relaxations of the molecules near the surface, which did not have a constraint in the *z*-axis.

3.1.2 *Density profile*

The density profiles (Figure 3) are shown as a function of the distance from the centre of the mass of the film. They are described by a hyperbolic tangent function of type

$$\rho(z) = \left(\frac{\rho_0}{2}\right)\left[1 - \tanh\left(\frac{z}{x_i}\right)\right], \qquad (2)$$

where ρ_0 is the bulk density and x_i is the calculated width of thin film (0.1 nm). The density of the film at its centre of mass was obtained as about 1.1–1.2 g cm^{-3} and this value was somewhat lower than the bulk density (BPDA-*m*-PDA: 1.25 ± 0.02 g cm^{-3}, BPDA-DABBE: 1.21 ± 0.02 g cm^{-3}, BPDA-DPA: 1.12 ± 0.03 g cm^{-3}). The density dropped at a distance of 1.0–1.2 nm from the surface, so the thickness of the simulated film was 2.0–2.4 nm, which was consistent with other simulation results in previous studies [27–29]. In the BPDA-DABBE and BPDA-DPA systems, the density decreased more slowly than in the BPDA-*m*-PDA system, as the side chain of the former two systems was emigrated in the surface region.

The proportions of the backbone and the side chain were examined. It was obvious that the side chain was rich at 0.5–1.0 nm from the surface, especially in the BPDA-DPA system (Figure 4), as the proportion was much higher than the averaged value. The XPS result also showed that the silicon content of the BPDA-DPA system was 3.11%, which was higher than its theoretic value for 1.96%.

3.1.3 *Surface configuration*

For aromatic PIs, the surface configuration is mainly determined by the arrangement of phenyl rings, and it is evaluated using the angle α, between the *z*-axis and the phenyl ring plane. The cosα is 1 if the phenyl ring is parallel with the *z*-axis, namely vertical to the *x*–*y* plane, and –1 if it is parallel with the *x*–*y* plane. The simulation results are presented in Figure 5. It could be deduced that the phenyl rings of BPDA-*m*-PDA were randomly arranged in the bulk for its large deviation of cosα, while being arranged parallel in the surface region because of its decrement in cosα compared with the bulk state. For the BPDA-DABBE system, its backbone were also parallel to the *x*–*y* plane in the surface region, while the side chain inclined to be arranged vertical to the *x*–*y* plane for comparatively larger cosα in the surface area. Moreover, the value of cosα in the surface area was even higher at 0.95 in the BPDA-DPA system, indicating that most of the phenyl rings in the surface area were vertical to the *x*–*y* plane. These results were in reasonable agreement with the experimental results [34]. The vertical configuration of the phenyl ring in the side chain of BPDA-DPA and BPDA-DABBE accounted for their high pretilt angles. A detailed discussion is given in Section 3.2.2.

To confirm that the orientation of the phenyl ring in the side chain was attributed to anisotropy in the *z*-axis, we examined the angle α, between the *y*-axis and the phenyl ring plane in the side chain of the BPDA-DPA system (Figure 6). With the increment of the

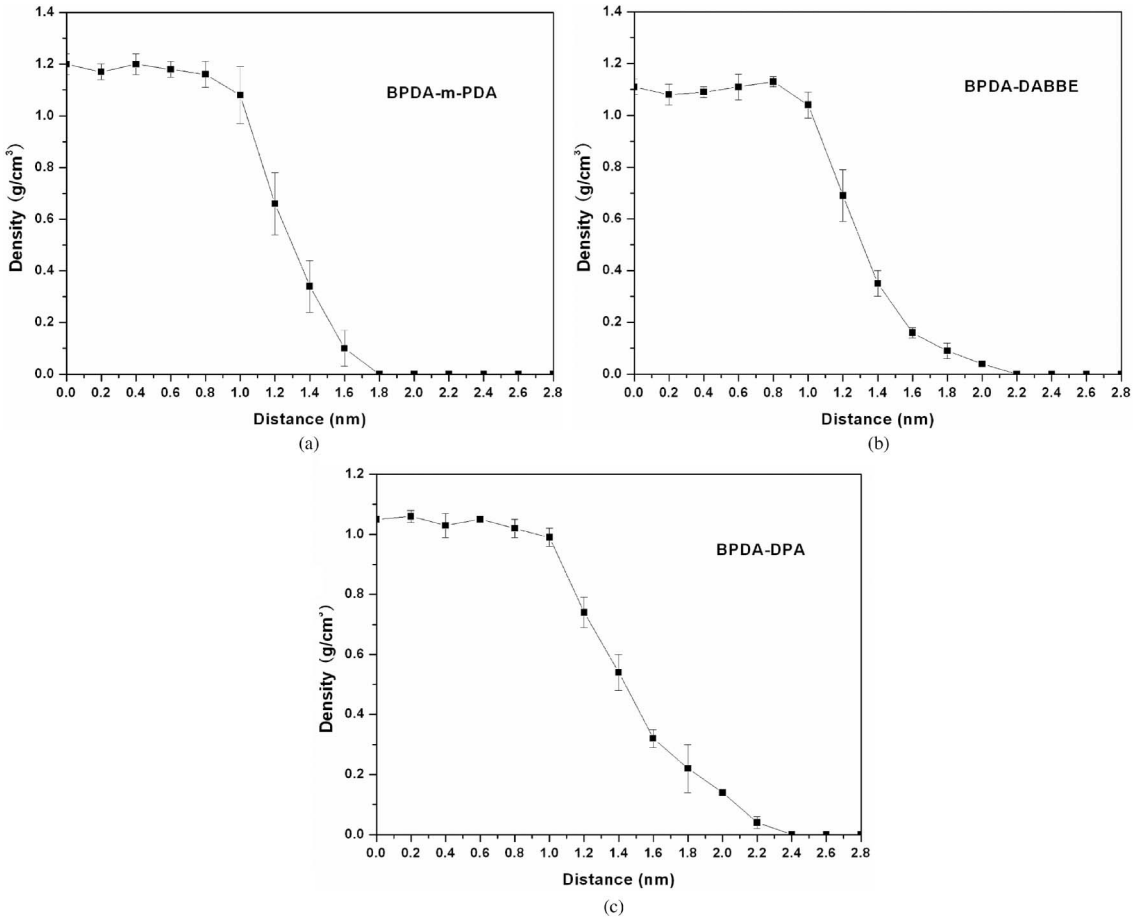

Figure 3. Density profile as a function of distance from the centre of mass for the three PI systems: (a) BPDA-*m*-PDA; (b) BPDA-DABBE; and (c) BPDA-DPA.

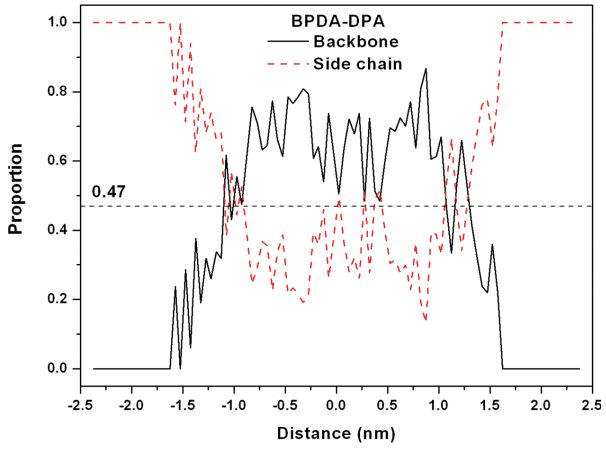

Figure 4. Proportion of backbone and side chain content along the *z*-axis versus the distance from the centre of mass in (a) BPDA-DABBE and (b) BPDA-DPA systems.

distance from the centre of mass, the change of cosα was not distinct and for the bulk state was maintained in the *y*-axis.

3.1.4 *Side chain mobility analysis*

To characterise the mobility of the polymer side chain, the auto-correlation time function (ACTF) could be calculated as

$$m_2(t) = 1.5<(u(t_0) \bullet u(t_0 + t))^2> - 0.5, \qquad (3)$$

where $u(t_0)$ and $u(t_0+ t)$ represent the unit vector at time t_0 and time $t_0 + t$, respectively. The angle bracket indicates an ensemble average over the same kind of vector along the polymer chain throughout the simulation time. At the same simulation time, the higher value of $m_2(t)$ represents the lesser mobility of the corresponding segments. We applied the optimal equilibrated configuration in the above MD simulation as an initial structure, and then calculated in the constant-*NVT* MD simulation for 2 ns. Only the initial 200 ps during this relaxation are shown [35].

The ACTF of BPDA-DABBE and BPDA-DPA in the bulk and film states were examined. In both two states, the BPDA-DABBE system decreased more

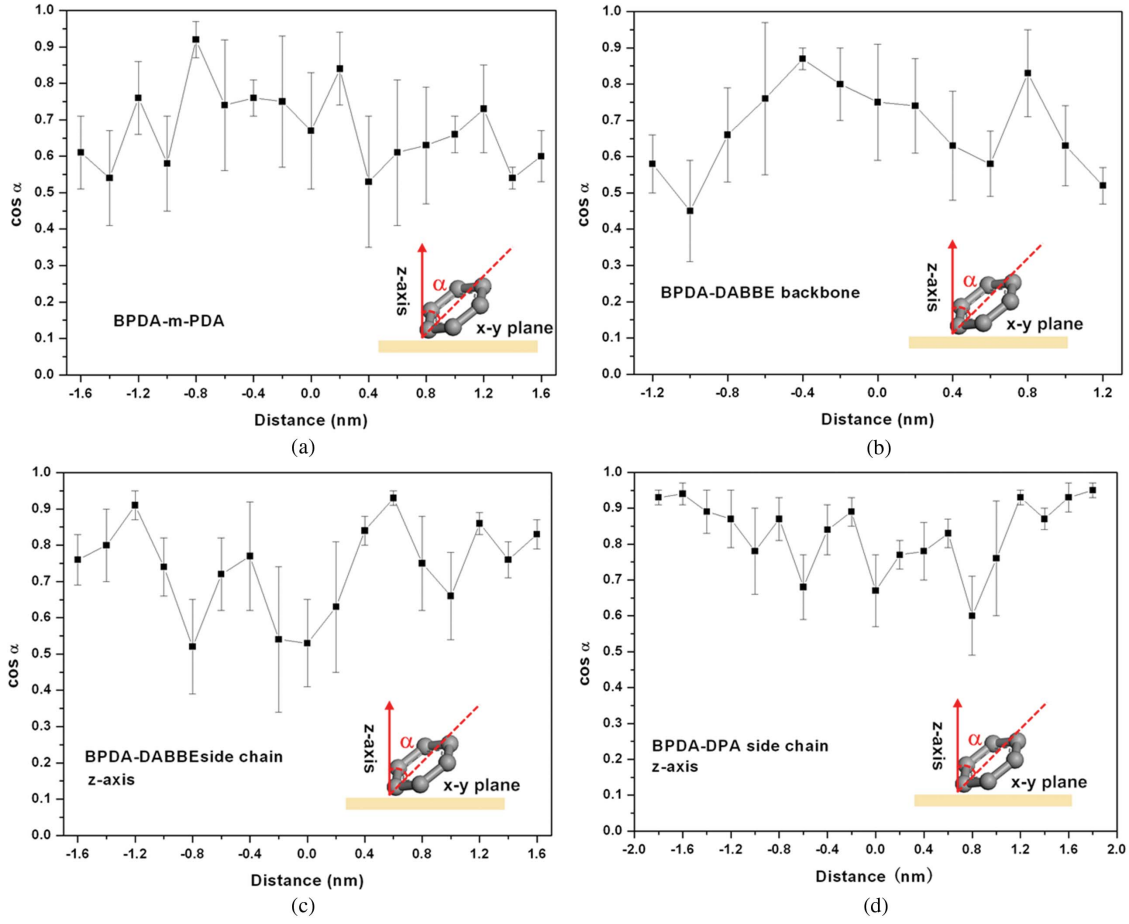

Figure 5. Plot of the angle between the phenyl ring in the PI systems and the *z*-axis versus the distance from the centre of the mass along the *z*-axis: (a) BPDA-*m*-PDA; (b) backbone; (c) side chain of BPDA-DABBE; and (d) side chain of BPDA-DPA.

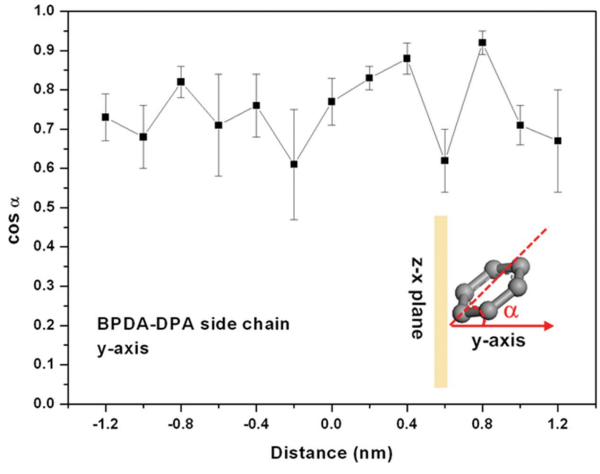

Figure 6. Plot of the angle between the phenyl ring of the side chain in the BPDA-DPA system and the *y*-axis versus the distance from the centre of the mass along the *y*-axis.

slowly than the BPDA-DPA system, indicating stronger rigidity of the side chain. The ACTF of the film decreased more dramatically than the bulk state, since the molecules in the surface area were easy to relax. This result has also been proven by the decreased bonded energy discussed in Section 3.1.1.

For a detailed BPDA-DABBE system, the side chain was divided into two parts (Figure 7): the 1 is the vector from C(sp) in the backbone diamine to C(sp) in the biphenyl group of side chain, the 2 is the vector from C(sp) that linked the carboxylic acid group in the side chain to the opposite C(sp) in the biphenyl group. From Figure 7(a), the two sets were stable in bulk, and the 1 was more stable due to the constraint from the backbone and the biphenyl group in side chain. However, both sets became more mobile for the relaxation of the side chain in the film state. Furthermore, the side chain of the BPDA-DPA system was divided into three parts (Figure 7(b)): the

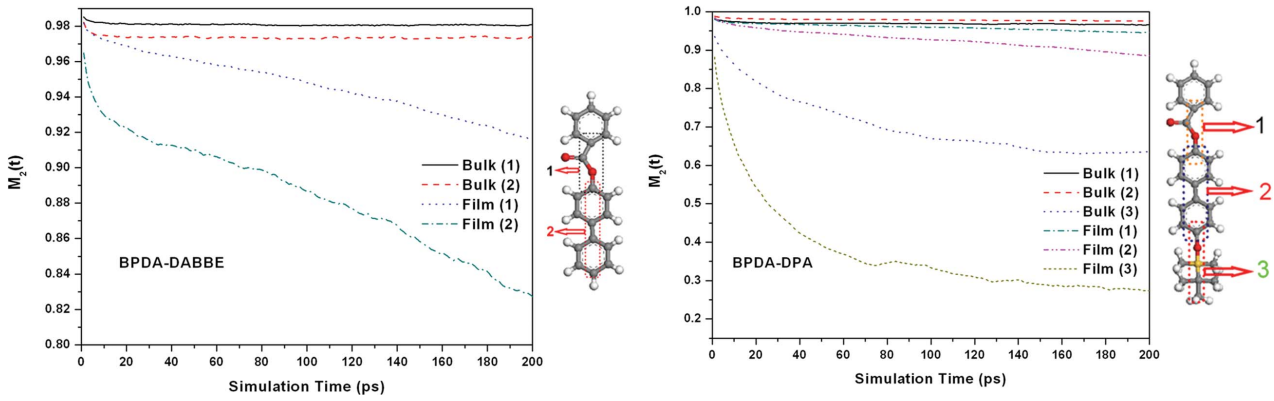

Figure 7. ACTFs for the bulk and film states of (a) BPDA-DABBE and (b) BPDA-DPA systems; 1, 2 and 3 are defined on the right of the figure.

1 and 2 are the same as the vectors in the BPDA-DPA system, the 3 is the vector from the end C(sp) in 2 to the C(sp3) in the end alkyl group. All three sets were more mobile in the film state; the 3 had much stronger mobility than the former two sets. The high mobility of the silyl group in the side chain could effectively help the side chain enrichment in the surface.

3.2 *Interactions between PI and the liquid crystal molecules*

3.2.1 *Orientation distribution function*

The orientation distribution function (ODF) was applied to study the pretilt angle of 5CB molecules on PI substrates. The core is defined as the vector of the mesogen group, namely the biphenyl group, and the tail is defined as the vector of the alkyl chain of the 5CB, from the C(sp3) linked to biphenyl group to the end C(sp3) in the alkyl chain. Figure 8 shows the ODFs of the 5CB core on PI substrates. The tilt angle greater than 90° corresponds to CN groups pointing up, and the angle less than 90° corresponds to CN groups pointing down. Therefore, the pretilt angle at the molecular scale can be defined as follows:

$$A_p = |A_t - 90°|, \tag{4}$$

where A_p is the pretilt angle and A_t is the tilt angle. Using this equation, the pretilt angles of the BPDA-*m*-PDA, BPDA-DABBE and BPDA-DPA systems were around 5°, 20° and 90°, which were consistent with the corresponding experimental values, that is 3°, 13° and 89°.

For BPDA-DABBE and BPDA-DPA systems, the proportion of tilt angles greater than 90° was greater than that of tilt angles less than 90°. In other words, the CN groups inclined to be in a pointed-down configuration, indicating that they preferred to contact with the PI backbone rather than the side chain. In all the three systems, the ODFs of alkyl tails in 5CB did not show a clear tilt angle because of the high mobility of the alkyl groups. The result is shown in Figure 8(d), using the BPDA-*m*-PDA system as an example.

The typical ODF for a monolayer of 5CB molecules with parallel starting configuration is shown in Figure 9. The ODF showed the same trend as the single molecule's ODF, but was widely distributed. The main reason was that the close packing effect made some LC molecules confine in a metastable state. Thus, they could not obtain the optimum configuration.

3.2.2 *Intermolecular interaction: density functional theory study*

The density functional theory (DFT) method, a popular quantum chemistry method involving accurate interactions at the atomic scale, was applied in order to study the interactions between 5CB and the PI monomer or side chain molecules [19]. The piecewise constant function [36, 37] with local density approximation was employed. The optimised molecular configurations of 5CB and the PI monomer or side chain molecules are shown in Figure 10. The common feature of these systems was that the biphenyl groups in 5CB were highly parallel arranged along the conjugated groups in the substrate. For the optimised molecular structure of the backbone PI monomer (Figure 10(a)) and DABBE side chain (Figure 10(b)), the distances from the centre of the biphenyl group in 5CB to the substrate were 0.342 nm and 0.344 nm, respectively. Similar arrangements are observed for the π–π interaction in biological systems, which indicated that this interaction also existed in our study [38]. Furthermore, the interaction energies between 5CB and the substrate were 78.7 kJ mol^{-1} (Figure 10(a)) and 76.0 kJ mol^{-1} (Figure 10(b)), which were much higher than common

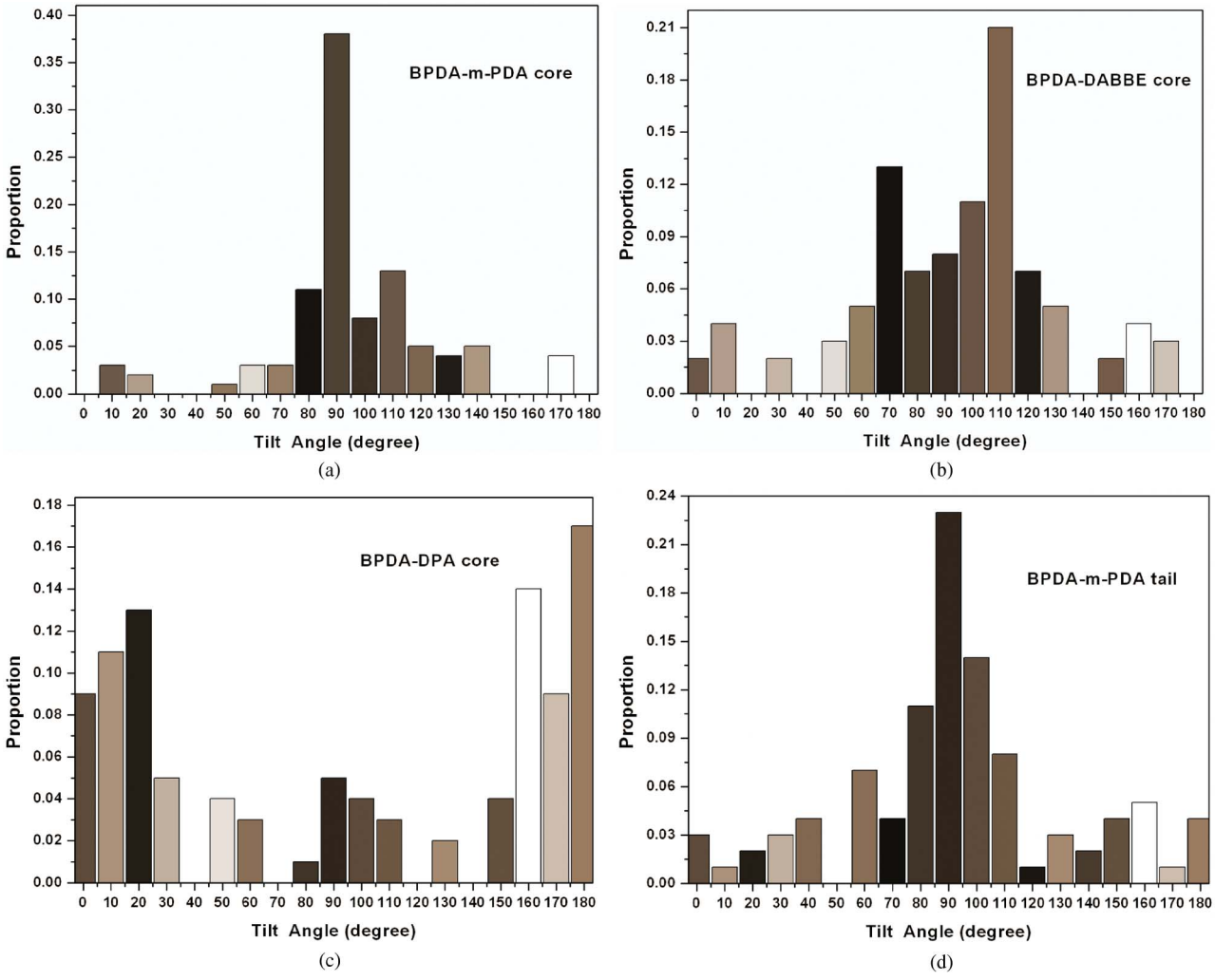

Figure 8. ODFs for a single 5CB molecule on PI substrates: the core of 5CB on (a) BPDA-*m*-PDA, (b) BPDA-DABBE, (c) BPDA-DPA, (d) the tail of 5CB on BPDA-*m*-PDA substrates.

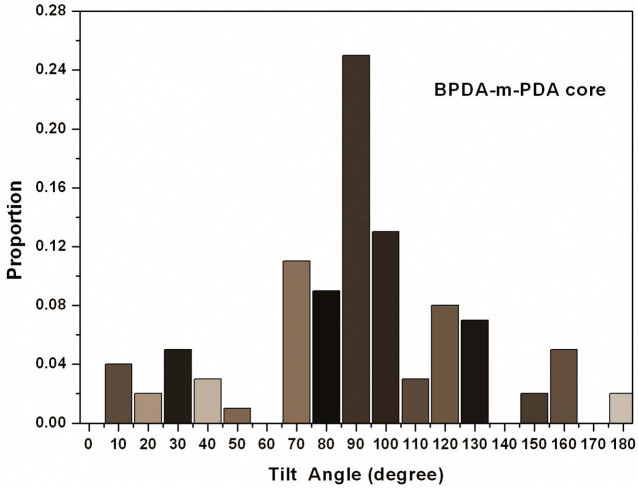

Figure 9. ODF for the core of the monolayer 5CB molecules on the BPDA-*m*-PDA substrate.

vdW forces (1–10 kJ mol^{-1}). Therefore, the main interaction between 5CB and the PI substrates were π–π interactions. The side chain of DPA had two configurations due to the direction of the angle of C-O-Si. The optimised molecular structure for when it pointed *up* is shown in Figure 10(c) and the *down* structure is shown in Figure 10(d). The distances from the centre of the biphenyl group in 5CB to the substrate in these two systems were 0.353 nm (Figure10(c)) and 0.368 nm (Figure 10(d)), which are larger than the counterparts in Figure 10(a) and (b). It was the steric effect of the DPA's silyl group that prevented the biphenyl group of 5CB to arrange parallel with DPA's side chain, and increased the distance between them to some extent. At the same time, the interaction energies decreased a little, which were 63.0 kJ mol^{-1} (Figure 10(c)) and 60.6 kJ mol^{-1} (Figure 10 (d)), respectively.

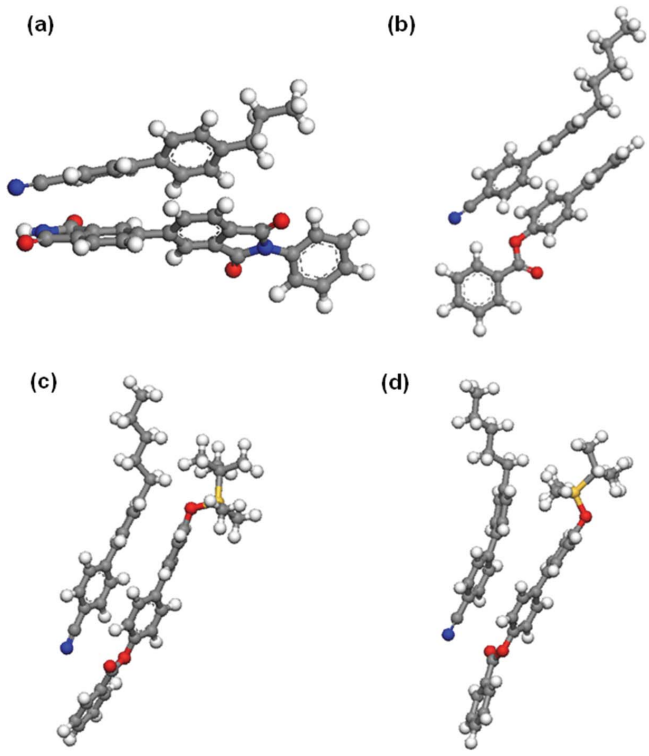

Figure 10. Optimised structures of 5CB and (a) BPDA/*m*-PDA, (b) DABBE (side chain), (c) DPA (side chain UP) and (d) DPA (side chain DOWN).

4. Conclusions

In order to study the effect of the biphenyl side chain structure of PI on the pretilt angle of LC cells, the surface properties of three PI systems were well examined. The density in the interior of the film was somewhat lower than the bulk density and dropped at a distance of 1.0–1.2 nm from the surface. The surface energy predicted by MD method showed a good agreement with the experimental result. The BPDA-DPA system had the lowest surface energy for the lowest decrease in non-bond energy. From ACTF studies, films showed higher mobility than the bulk states in all the PI systems, especially in the BPDA-DPA system. The main reason for this was the high mobility of the silyl group in its side chain. The phenyl ring of BPDA-*m*-PDA was randomly arranged in the bulk, while being inclined to be parallel in the surface region. The backbones of the BPDA-DABBE and BPDA-DPA systems were also apt to be parallel to the *x*–*y* plane in the surface region, yet their side chains were inclined to be vertical to the *x*–*y* plane. The pretilt angles of the BPDA-*m*-PDA, BPDA-DABBE and BPDA-DPA systems by a single 5CB simulation were around 5°, 20° and 90°, which were comparable to the experimental values of 3°, 13° and 89°. The alkyl tail in 5CB could not orient well for its high mobility. The monolayer 5CB molecule ODFs showed the same trend as the single-molecule result, but were distributed widely because of the close packing effect. The 5CB molecules were arranged parallel along the conjugated groups in the substrate. Due to the steric effect of the silyl end group, the biphenyl group of the 5CB could not be well arranged in parallel on the DPA's side chain and it decreased the interaction energy a little.

The main mechanism for 5CB molecules' alignment on the PI substrate was the π–π interaction between biphenyl groups. The high pretilt angle of the BPDA-DPA system was accounted for by the vertical configuration of the phenyl ring and the silyl group, as this could fix the configuration of the 5CB molecules and increase the pretilt angle at the same time.

Acknowledgements

We are grateful for the financial support from the National Natural Science Foundation of China (No.50433010) and the Doctoral Fund of Ministry of Education of China (No.20040610028).

References

[1] Choi, K.-Y.; Lee, B.J.; Yi, M.H.; Kim, H.K. *Mol. Cryst. Liq. Cryst.* **2000**, *353*, 355–371.
[2] Takatoh, K.; Sakamoto, M.; Hasegawa, R.; Koden, M.; Itoh, N.; Hasegawa, M. *Alignment Technologies and Applications of Liquid Crystal Devices*; Taylor & Francis: London, 2005.
[3] Gibbons, W.M.; Shannon, P.J.; Sun, S.-T.; Swetlin, B.J. *Nature*, **1991**, *351*, 49–50.
[4] Chigrinov, V.G.; Kozenkov, V.M.; Kwok, H-S. *Photoalignment of Liquid Crystalline Materials: Physics and Applications*; Wiley: New York, 2008.
[5] Lee, Y.J.; Choi, J.G.; Song, I.; Oh, J.M.; Yi, M.H. *Polymer* **2006**, *47*, 1555–1561.
[6] Paek, S.H.; Durning, C.J.; Lee, K.W; Lien, A. *J. Appl. Phys.* **1998**, *83*, 1270–1280.
[7] Ban, B.S.; Rim, Y.N.; Kim, Y.B. *Liquid Crystals* **2000**, *27*, 125–130.
[8] Sarkar, A.; More, A.S.; Wadgaonkar, P.P.; Shin, G.J.; Jung J.C. *J. Appl. Polym. Sci.* **2007**, *105*, 1793–1801.
[9] Li, L.; Yin. J.; Xu, H.-J.; Fang, J.-H; Zhu, Z.-K; Wang, Z.-G. *J. Polym. Sci., Part A: Polym. Chem.* **2000**, *38*, 1943–1950.
[10] Liu, J.G.; Li, Z.X.; Wu, J.T.; Zhou, H.W.; Wang, F.S.; Yang, S.Y. *J. Polym. Sci., Part A: Polym. Chem.* **2002**, *40*, 1583–1593.
[11] Chae, B.; Kim, S.B.; Lee, S.W.; Kim, S.I.; Choi, W.; Lee, B.; Ree, M.; Lee, K.H.; Jung, J.C. *Macromolecules* **2002**, *35*, 10119–10130.
[12] Lee, S.W.; Lee, S.J.; Hahm, S.G.; Lee, T.J.; Lee, B.; Chae, B.; Kim, S.B.; Jung, J.C.; Zin, W.-C.; Sohn, B.-H.; Ree, M. *Macromolecules* **2005**, *38*, 4331–4338.
[13] Lee, S.B.; Shin, G.J.; Chi, J.H.; Zin, W.C.; Jung, J.C.; Hahm, S.G.; Ree, M.; Chang, T. *Polymer* **2006**, *47*, 6606–6621.

[14] Liu, Z.; Yu, F.; Zhang, Q.; Zeng, Y.; Wang, Y. *Eur. Polym. J.* **2008**, *44*, 2718–2727.
[15] Lai, H.; Qin, L.; Liu, X.Y.; Gu, Y. *Eur. Polym. J.* **2008**, *44*, 3724–3731.
[16] Yoneya, M.; Iwakabe, Y. *Liquid Crystals* **1995**, *21*, 347–359.
[17] Liu, X.Y.; Xu, W.; Ye, G.D.; Gu, Y. *Polym. Eng. Sci.* **2006**, *46*, 123–128.
[18] Lai, H.; Liu, X.; Qin, L.; Li, M.; Gu, Y. *Liquid Crystals* **2009**, *36*, 173–178.
[19] Materials Studio software. http://www.acclerys.com (accessed July 22, 2009).
[20] Mayo, S.L.; Olafson, B.D.; Goddard, W.A. *J. Phys. Chem.* **1990**, *94*, 8897–8909.
[21] Fan, C.F.; Cagin, T.; Chen, Z.M.; Smith, K.A. *Macromolecules* **1994**, *27*, 2383–2391.
[22] Pan, R.; Liu, X.; Zhang, A.; Gu, Y. *Comput. Mater. Sci.* **2007**, *39*, 887–895.
[23] Theodorou, D.N.; Suter, U.W. *Macromolecules* **1985**, *18*, 1467–1478.
[24] Theodorou, D.N.; Suter, U.W. *Macromolecules* **1986**, *19*, 139–154.
[25] Kang, J.W.; Choi, K.; Jo, W.H.; Hsu, S.L. *Polymer* **1998**, *39*, 7079–7087.
[26] Sanghun, L.; Jaeeon, C.; Richard, L.J.; Do, Y.Y. *Macromolecules* **2007**, *40*, 7407–7412.
[27] Prathab, B.; Aminabhavi, T.M. *Langmuir* **2007**, *23*, 5439–5444.
[28] Ijantkar, A.S.; Natarajan, U. *Polymer* **2004**, *45*, 1373–1381.
[29] Natarajan, U.; Tanaka, G.; Mattice, W.L. *J. Comput. Aided Mater. Des.* **1997**, *4*, 193–205.
[30] Binger, D.R.; Hanna, S. *Liquid Crystals* **1999**, *26*, 1205–1224.
[31] Nosé, S. *Mol. Phys.* **1984**, *52*, 255–268.
[32] Nosé, S. *J. Chem. Phys.* **1984**, *81*, 511–519.
[33] Berendsen, H.J.C.; Postma, J.P.M.; van Gunsteren, W.F.; DiNola, A.; Haak, J.R. *J. Chem. Phys.* **1984**, *81*, 3684–3690.
[34] Stöhr, M.; Samant, M.G.; Cossy-Favre, A.; Diaz, J.; Momoi, Y.; Odahara, S.; Nagata, T. *Macromolecules* **1998**, *31*, 1942–1946.
[35] Wu, C.; Xu, W. *Polymer* **2007**, *48*, 5802–5812.
[36] Perdew, J.P.; Wang, Y. *Phys. Rev. B* **1992**, *45*, 13244–13249.
[37] Perdew, J.P.; Wang. Y. *Phys. Rev. B* **1986**, *33*, 8800–8802.
[38] Ranganathan, D.; Haridas, V.; Gilardi, R.; Karle, I.L. *J. Am. Chem. Soc.* **1998**, *120*, 10793–10800.